From Figures 4.10 and 4.11, we have

α	c_ℓ	c_d	c_ℓ/c_d
0	0.25	0.0065	38.5
4	0.65	0.0070	93
8	1.08	0.0112	96
12	1.44	0.017	85

Note that, as the angle of attack increases, the lift-to-drag ratio first increases, reaches a maximum, and then decreases. The maximum lift-to-drag ratio, $(L/D)_{\max}$, is an important parameter in airfoil performance; it is a direct measure of aerodynamic efficiency. The higher the value of $(L/D)_{\max}$, the more efficient is the airfoil. The values of L/D for airfoils are quite large numbers in comparison to that for a complete airplane. Due to the extra drag associated with all parts of the airplane, values of $(L/D)_{\max}$ for real airplanes are on the order of 10 to 20.

4.4 PHILOSOPHY OF THEORETICAL SOLUTIONS FOR LOW-SPEED FLOW OVER AIRFOILS: THE VORTEX SHEET

In Section 3.14, the concept of vortex flow was introduced; refer to Figure 3.31 for a schematic of the flow induced by a point vortex of strength Γ located at a given point O. (Recall that Figure 3.31, with its counterclockwise flow, corresponds to a negative value of Γ. By convention, a positive Γ induces a clockwise flow.) Let us now expand our concept of a point vortex. Referring to Figure 3.31, imagine a straight line perpendicular to the page, going through point O, and extending to infinity both out of and into the page. This line is a straight *vortex filament* of strength Γ. A straight vortex filament is drawn in perspective in Figure 4.12. (Here, we show a clockwise flow, which corresponds to a positive value of Γ.) The flow induced in any plane perpendicular to the straight vortex filament by the filament itself is identical to that induced by a point vortex of strength Γ; that is, in Figure 4.12, the flows in the planes perpendicular to the vortex filament at O and O' are identical to each other and are identical to the flow induced by a point vortex of strength Γ. Indeed, the point vortex described in Section 3.14 is simply a section of a straight vortex filament.

In Section 3.17, we introduced the concept of a source sheet, which is an infinite number of line sources side by side, with the strength of each line source being infinitesimally small. For vortex flow, consider an analogous situation. Imagine an infinite number of straight vortex filaments side by side, where the strength of each filament is infinitesimally small. These side-by-side vortex filaments form a *vortex sheet,* as shown in perspective in the upper left of Figure 4.13. If we look along the series of vortex filaments (looking along the y axis in Figure 4.13), the vortex sheet will appear as sketched at the lower right of Figure 4.13. Here, we are looking at an edge view of the sheet; the vortex filaments are all perpendicular

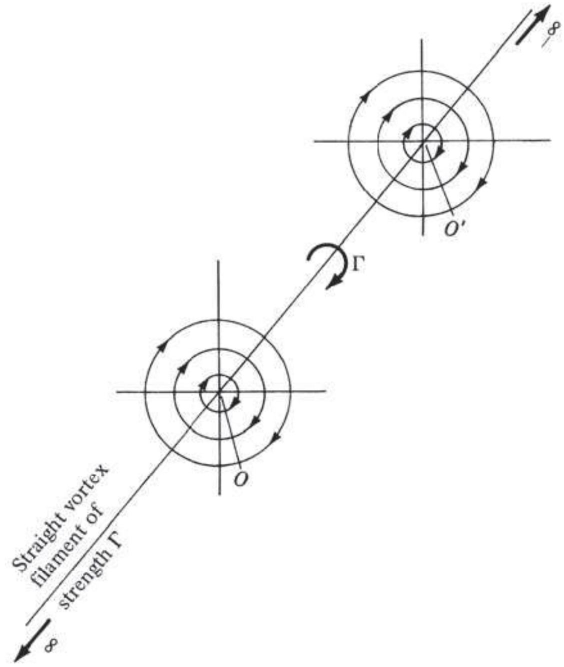

Figure 4.12 Vortex filament.

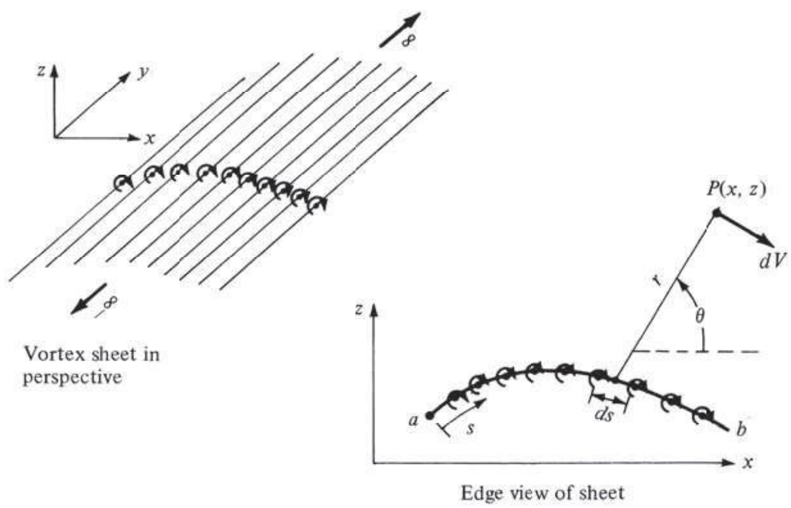

Figure 4.13 Vortex sheet.

to the page. Let s be the distance measured along the vortex sheet in the edge view. Define $\gamma = \gamma(s)$ as the strength of the vortex sheet, per unit length along s. Thus, the strength of an infinitesimal portion ds of the sheet is $\gamma\, ds$. This small section of the vortex sheet can be treated as a distinct vortex of strength $\gamma\, ds$. Now consider point P in the flow, located a distance r from ds; the cartesian coordinates of P are (x, z). The small section of the vortex sheet of strength $\gamma\, ds$ induces an infinitesimally small velocity dV at point P. From Equation (3.105), dV is given by

$$dV = -\frac{\gamma\, ds}{2\pi r} \tag{4.1}$$

and is in a direction perpendicular to r, as shown in Figure 4.13. The velocity at P induced by the entire vortex sheet is the summation of Equation (4.1) from point a to point b. Note that dV, which is perpendicular to r, changes direction at point P as we sum from a to b; hence, the incremental velocities induced at P by different sections of the vortex sheet must be added vectorally. Because of this, it is sometimes more convenient to deal with the velocity potential. Again referring to Figure 4.13, the increment in velocity potential $d\phi$ induced at point P by the elemental vortex $\gamma\, ds$ is, from Equation (3.112),

$$d\phi = -\frac{\gamma\, ds}{2\pi}\theta \tag{4.2}$$

In turn, the velocity potential at P due to the entire vortex sheet from a to b is

$$\boxed{\phi(x, z) = -\frac{1}{2\pi}\int_a^b \theta\gamma\, ds} \tag{4.3}$$

Equation (4.1) is particularly useful for our discussion of classical thin airfoil theory, whereas Equation (4.3) is important for the numerical vortex panel method.

Recall from Section 3.14 that the circulation Γ around a point vortex is equal to the strength of the vortex. Similarly, the circulation around the vortex sheet in Figure 4.13 is the sum of the strengths of the elemental vortices; that is,

$$\boxed{\Gamma = \int_a^b \gamma\, ds} \tag{4.4}$$

Recall that the source sheet introduced in Section 3.17 has a discontinuous change in the direction of the *normal* component of velocity across the sheet (from Figure 3.38, note that the normal component of velocity changes direction by 180° in crossing the sheet), whereas the tangential component of velocity is the same immediately above and below the source sheet. In contrast, for a vortex sheet, there is a discontinuous change in the tangential component of velocity across the sheet, whereas the normal component of velocity is preserved across the sheet. This change in tangential velocity across the vortex sheet is related to the strength of the sheet as follows. Consider a vortex sheet as sketched in

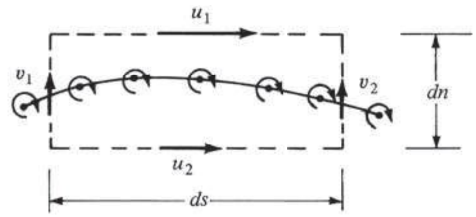

Figure 4.14 Tangential velocity jump across a vortex sheet.

Figure 4.14. Consider the rectangular dashed path enclosing a section of the sheet of length ds. The velocity components tangential to the top and bottom of this rectangular path are u_1 and u_2, respectively, and the velocity components tangential to the left and right sides are v_1 and v_2, respectively. The top and bottom of the path are separated by the distance dn. From the definition of circulation given by Equation (2.136), the circulation around the dashed path is

$$\Gamma = -(v_2\,dn - u_1\,ds - v_1\,dn + u_2\,ds)$$

or

$$\Gamma = (u_1 - u_2)\,ds + (v_1 - v_2)\,dn \tag{4.5}$$

However, since the strength of the vortex sheet contained inside the dashed path is $\gamma\,ds$, we also have

$$\Gamma = \gamma\,ds \tag{4.6}$$

Therefore, from Equations (4.5) and (4.6),

$$\gamma\,ds = (u_1 - u_2)\,ds + (v_1 - v_2)\,dn \tag{4.7}$$

Let the top and bottom of the dashed line approach the vortex sheet; that is, let $dn \to 0$. In the limit, u_1 and u_2 become the velocity components tangential to the vortex sheet immediately above and below the sheet, respectively, and Equation (4.7) becomes

$$\gamma\,ds = (u_1 - u_2)\,ds$$

or

$$\boxed{\gamma = u_1 - u_2} \tag{4.8}$$

Equation (4.8) is important; it states that *the local jump in tangential velocity across the vortex sheet is equal to the local sheet strength.*

We have now defined and discussed the properties of a vortex sheet. The concept of a vortex sheet is instrumental in the analysis of the low-speed characteristics of an airfoil. A philosophy of airfoil theory of inviscid, incompressible flow is as follows. Consider an airfoil of arbitrary shape and thickness in a freestream with velocity V_∞, as sketched in Figure 4.15. Replace the airfoil surface with a vortex sheet of variable strength $\gamma(s)$, as also shown in Figure 4.15. Calculate the variation of γ as a function of s such that the induced velocity field from the vortex sheet when added to the uniform velocity of magnitude V_∞ will make

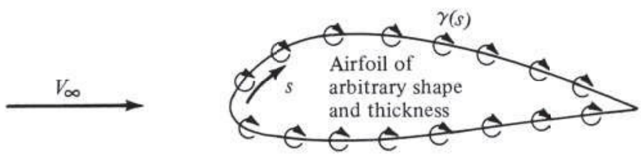

Figure 4.15 Simulation of an arbitrary airfoil by distributing a vortex sheet over the airfoil surface.

the vortex sheet (hence the airfoil surface) a *streamline of the flow*. In turn, the circulation around the airfoil will be given by

$$\Gamma = \int \gamma \, ds$$

where the integral is taken around the complete surface of the airfoil. Finally, the resulting lift is given by the Kutta-Joukowski theorem:

$$L' = \rho_\infty V_\infty \Gamma$$

This philosophy is not new. It was first espoused by Ludwig Prandtl and his colleagues at Göttingen, Germany, during the period 1912–1922. However, no general analytical solution for $\gamma = \gamma(s)$ exists for an airfoil of arbitrary shape and thickness. Rather, the strength of the vortex sheet must be found numerically, and the practical implementation of the above philosophy had to wait until the 1960s with the advent of large digital computers. Today, the above philosophy is the foundation of the modern vortex panel method, to be discussed in Section 4.9.

The concept of replacing the airfoil surface in Figure 4.15 with a vortex sheet is more than just a mathematical device; it also has physical significance. In real life, there is a thin boundary layer on the surface, due to the action of friction between the surface and the airflow (see Figures 1.41 and 1.46). This boundary layer is a highly viscous region in which the large velocity gradients produce substantial vorticity; that is, $\nabla \times \mathbf{V}$ is finite within the boundary layer. (Review Section 2.12 for a discussion of vorticity.) Hence, in real life, there is a distribution of vorticity along the airfoil surface due to viscous effects, and our philosophy of replacing the airfoil surface with a vortex sheet (such as in Figure 4.15) can be construed as a way of modeling this effect in an inviscid flow.[3]

Imagine that the airfoil in Figure 4.15 is made very thin. If you were to stand back and look at such a thin airfoil from a distance, the portions of the vortex sheet

[3] It is interesting to note that some recent research by NASA is hinting that even as complex a problem as flow separation, heretofore thought to be a completely viscous-dominated phenomenon, may in reality be an inviscid-dominated flow which requires only a rotational flow. For example, some inviscid flow-field numerical solutions for flow over a circular cylinder, when vorticity is introduced either by means of a nonuniform freestream or a curved shock wave, are accurately predicting the separated flow on the rearward side of the cylinder. However, as exciting as these results may be, they are too preliminary to be emphasized in this book. We continue to talk about flow separation in Chapters 15 to 20 as being a viscous-dominated effect, until definitely proved otherwise. This recent research is mentioned here only as another example of the physical connection between vorticity, vortex sheets, viscosity, and real life.

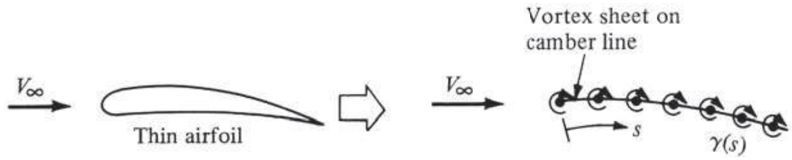

Figure 4.16 Thin airfoil approximation.

on the top and bottom surface of the airfoil would almost coincide. This gives rise to a method of approximating a thin airfoil by replacing it with a single vortex sheet distributed over the camber line of the airfoil, as sketched in Figure 4.16. The strength of this vortex sheet $\gamma(s)$ is calculated such that, in combination with the freestream, the camber line becomes a streamline of the flow. Although the approach shown in Figure 4.16 is approximate in comparison with the case shown in Figure 4.15, it has the advantage of yielding a closed-form analytical solution. This philosophy of thin airfoil theory was first developed by Max Munk, a colleague of Prandtl, in 1922 (see Reference 12). It is discussed in Sections 4.7 and 4.8.

4.5 THE KUTTA CONDITION

The lifting flow over a circular cylinder was discussed in Section 3.15, where we observed that an infinite number of potential flow solutions were possible, corresponding to the infinite choice of Γ. For example, Figure 3.33 illustrates three different flows over the cylinder, corresponding to three different values of Γ. The same situation applies to the potential flow over an airfoil; for a given airfoil at a given angle of attack, there are an infinite number of valid theoretical solutions, corresponding to an infinite choice of Γ. For example, Figure 4.17 illustrates two different flows over the same airfoil at the same angle of attack but with different values of Γ. At first, this may seem to pose a dilemma. We know from experience that a given airfoil at a given angle of attack produces a single value of lift (e.g., see Figure 4.10). So, although there is an infinite number of possible potential flow solutions, nature knows how to pick a particular solution. Clearly, the philosophy discussed in the previous section is not complete—we need an additional condition that *fixes* Γ for a given airfoil at a given α.

To attempt to find this condition, let us examine some experimental results for the development of the flow field around an airfoil which is set into motion from an initial state of rest. Figure 4.18 shows a series of classic photographs of the flow over an airfoil, taken from Prandtl and Tietjens (Reference 8). In Figure 4.18*a*, the flow has just started, and the flow pattern is just beginning to develop around the airfoil. In these early moments of development, the flow tries to curl around the sharp trailing edge from the bottom surface to the top surface, similar to the sketch shown at the left of Figure 4.17. However, more advanced considerations of inviscid, incompressible flow (see, e.g., Reference 9) show the theoretical result that the velocity becomes infinitely large at a sharp corner. Hence, the type

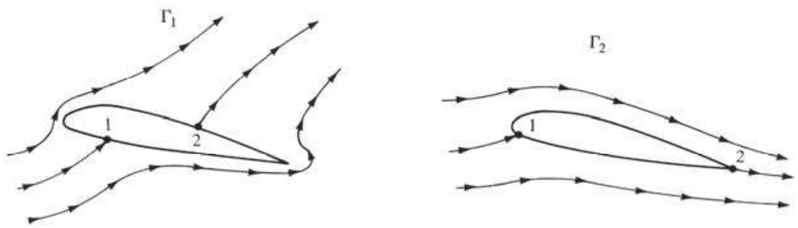

Figure 4.17 Effect of different values of circulation on the potential flow over a given airfoil at a given angle of attack. Points 1 and 2 are stagnation points.

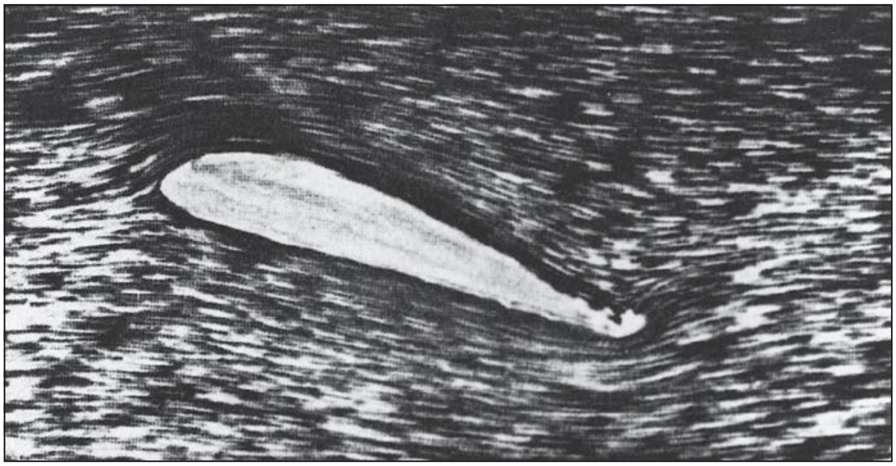

(*a*)

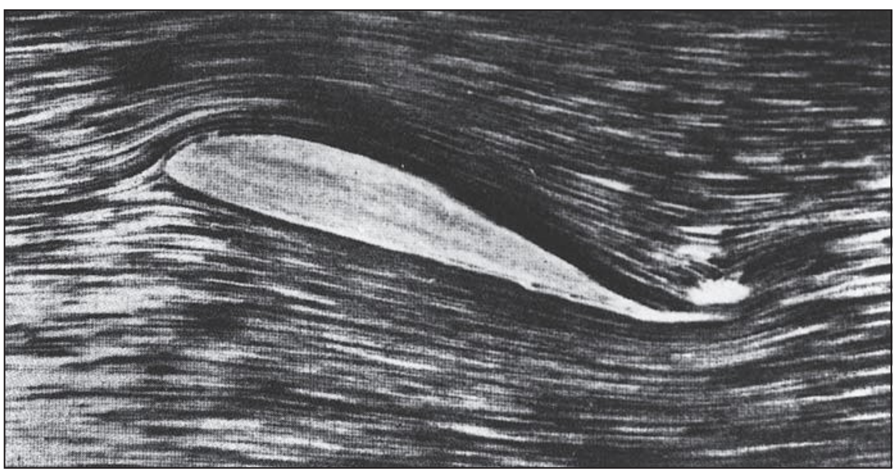

(*b*)

Figure 4.18 The development of steady flow over an airfoil; the airfoil is impulsively started from rest and attains a steady velocity through the fluid. (*a*) A moment just after starting. (*b*) An intermediate time. (Both photos: Prandtl, L., and O. G. Tietjens: *Applied Hydro and Aeromechanics Based on Lectures of L. Prandtl*, United Engineering Trustees Inc.,1934, McGraw-Hill, New York.)

(*c*)

Figure 4.18 (*continued*) The development of steady flow over an airfoil; the airfoil is impulsively started from rest and attains a steady velocity through the fluid. (*c*) The final steady flow. (Prandtl, L., and O. G. Tietjens: *Applied Hydro and Aeromechanics Based on Lectures of L. Prandtl*, United Engineering Trustees Inc.,1934, McGraw-Hill, New York.)

of flow sketched at the left of Figure 4.17, and shown in Figure 4.18*a*, is not tolerated very long by nature. Rather, as the real flow develops over the airfoil, the stagnation point on the upper surface (point 2 in Figure 4.17) moves toward the trailing edge. Figure 4.18*b* shows this intermediate stage. Finally, after the initial transient process dies out, the steady flow shown in Figure 4.18*c* is reached. This photograph demonstrates that the flow is *smoothly leaving the top and the bottom surfaces of the airfoil at the trailing edge*. This flow pattern is sketched at the right of Figure 4.17 and represents the type of pattern to be expected for the steady flow over an airfoil.

Reflecting on Figures 4.17 and 4.18, we emphasize again that in establishing the steady flow over a given airfoil at a given angle of attack, nature adopts that particular value of circulation (Γ_2 in Figure 4.17) which results in the flow leaving smoothly at the trailing edge. This observation was first made and used in a theoretical analysis by the German mathematician M. Wilhelm Kutta in 1902. Therefore, it has become known as the *Kutta condition*.

In order to apply the Kutta condition in a theoretical analysis, we need to be more precise about the nature of the flow at the trailing edge. The trailing edge can have a finite angle, as shown in Figures 4.17 and 4.18 and as sketched at the left of Figure 4.19, or it can be cusped, as shown at the right of Figure 4.19. First, consider the trailing edge with a finite angle, as shown at the left of Figure 4.19. Denote the velocities along the top surface and the bottom surface as V_1 and V_2, respectively. V_1 is parallel to the top surface at point a, and V_2 is parallel to the bottom surface at point a. For the finite-angle trailing edge, if these velocities were

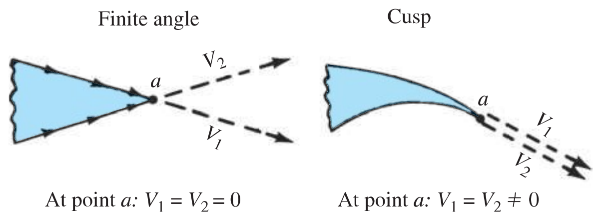

Figure 4.19 Different possible shapes of the trailing edge and their relation to the Kutta condition.

finite at point a, then we would have two velocities in two different directions at the same point, as shown at the left of Figure 4.19. However, this is not physically possible, and the only recourse is for both V_1 and V_2 to be zero at point a. That is, for the finite trailing edge, point a is a stagnation point, where $V_1 = V_2 = 0$. In contrast, for the cusped trailing edge shown at the right of Figure 4.19, V_1 and V_2 are in the same direction at point a, and hence both V_1 and V_2 can be finite. However, the pressure at point a, p_2, is a single, unique value, and Bernoulli's equation applied at both the top and bottom surfaces immediately adjacent to point a yields

$$p_a + \tfrac{1}{2}\rho V_1^2 = p_a + \tfrac{1}{2}\rho V_2^2$$

or

$$V_1 = V_2$$

Hence, for the cusped trailing edge, we see that the velocities leaving the top and bottom surfaces of the airfoil at the trailing edge are finite and equal in magnitude and direction.

We can summarize the statement of the Kutta condition as follows:

1. For a given airfoil at a given angle of attack, the value of Γ around the airfoil is such that the flow leaves the trailing edge smoothly.
2. If the trailing-edge angle is finite, then the trailing edge is a stagnation point.
3. If the trailing edge is cusped, then the velocities leaving the top and bottom surfaces at the trailing edge are finite and equal in magnitude and direction.

Consider again the philosophy of simulating the airfoil with vortex sheets placed either on the surface or on the camber line, as discussed in Section 4.4. The strength of such a vortex sheet is variable along the sheet and is denoted by $\gamma(s)$. The statement of the Kutta condition in terms of the vortex sheet is as follows. At the trailing edge (TE), from Equation (4.8), we have

$$\gamma(\text{TE}) = \gamma(a) = V_1 - V_2 \tag{4.9}$$

However, for the finite-angle trailing edge, $V_1 = V_2 = 0$; hence, from Equation (4.9), $\gamma(\text{TE}) = 0$. For the cusped trailing edge, $V_1 = V_2 \neq 0$; hence, from Equation (4.9), we again obtain the result that $\gamma(\text{TE}) = 0$. Therefore, the Kutta condition expressed in terms of the strength of the vortex sheet is

$$\boxed{\gamma(\text{TE}) = 0} \tag{4.10}$$

4.5.1 Without Friction Could We Have Lift?

In Section 1.5 we emphasized that the resultant aerodynamic force on a body immersed in a flow is due to the net integrated effect of the pressure and shear stress distributions over the body surface. Moreover, in Section 4.1 we noted that lift on an airfoil is primarily due to the surface pressure distribution, and that shear stress has virtually no effect on lift. It is easy to see why. Look at the airfoil shapes in Figures 4.17 and 4.18, for example. Recall that pressure acts *normal* to the surface, and for these airfoils the direction of this normal pressure is essentially in the vertical direction, that is, the lift direction. In contrast, the shear stress acts *tangential* to the surface, and for these airfoils the direction of this tangential shear stress is mainly in the horizontal direction, that is, the drag direction. Hence, pressure is the dominant player in the generation of lift, and shear stress has a negligible effect on lift. It is for this reason that the lift on an airfoil below the stall can be accurately predicted by *inviscid* theories such as that discussed in this chapter.

However, if we lived in a perfectly inviscid world, an airfoil could not produce lift. Indeed, the presence of friction is the very reason why we have lift. These sound like strange, even contradictory statements to our discussion in the preceding paragraph. What is going on here? The answer is that in real life, the *way* that nature insures that the flow will leave smoothly at the trailing edge, that is, the mechanism that nature uses to choose the flow shown in Figure 4.18*c*, is that the viscous boundary layer remains attached to the surface all the way to the trailing edge. *Nature enforces the Kutta condition by means of friction*. If there were no boundary layer (i.e., no friction), there would be no physical mechanism in the real world to achieve the Kutta condition.

So we are led to the most ironic situation that lift, which is created by the surface pressure distribution—an inviscid phenomenon, would not exist in a frictionless (inviscid) world. In this regard, we can say that without friction we could not have lift. However, we say this in the informed manner as discussed above.

4.6 KELVIN'S CIRCULATION THEOREM AND THE STARTING VORTEX

In this section, we put the finishing touch to the overall philosophy of airfoil theory before developing the quantitative aspects of the theory itself in subsequent sections. This section also ties up a loose end introduced by the Kutta condition described in the previous section. Specifically, the Kutta condition states that the circulation around an airfoil is just the right value to ensure that the flow smoothly leaves the trailing edge. *Question:* How does nature generate this circulation?

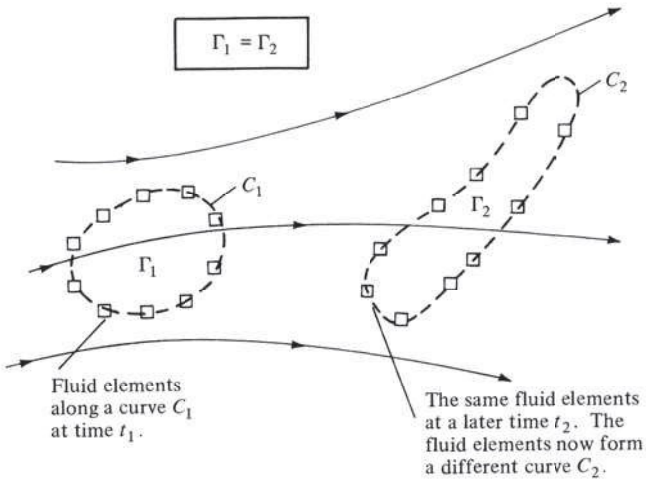

Figure 4.20 Kelvin's theorem.

Does it come from nowhere, or is circulation somehow conserved over the whole flow field? Let us examine these matters more closely.

Consider an arbitrary inviscid, incompressible flow as sketched in Figure 4.20. Assume that all body forces **f** are zero. Choose an arbitrary curve C_1 and identify the fluid elements that are on this curve at a given instant in time t_1. Also, by definition the circulation around curve C_1 is $\Gamma_1 = -\int_{C_1} \mathbf{V} \cdot \mathbf{ds}$. Now let these specific fluid elements move downstream. At some later time, t_2, these *same* fluid elements will form another curve C_2, around which the circulation is $\Gamma_2 = -\int_{C_2} \mathbf{V} \cdot \mathbf{ds}$. For the conditions stated above, we can readily show that $\Gamma_1 = \Gamma_2$. In fact, since we are following a set of specific fluid elements, we can state that circulation around a closed curve formed by a set of contiguous fluid elements remains constant as the fluid elements move throughout the flow. Recall from Section 2.9 that the substantial derivative gives the time rate of change following a given fluid element. Hence, a mathematical statement of the above discussion is simply

$$\boxed{\frac{D\Gamma}{Dt} = 0} \tag{4.11}$$

which says that the time rate of change of circulation around a closed curve consisting of the same fluid elements is zero. Equation (4.11) along with its supporting discussion is called *Kelvin's circulation theorem*.[4] Its derivation from

[4] Kelvin's theorem also holds for an inviscid compressible flow in the special case where $\rho = \rho(p)$; that is, the density is some single-valued function of pressure. Such is the case for isentropic flow, to be treated in later chapters.

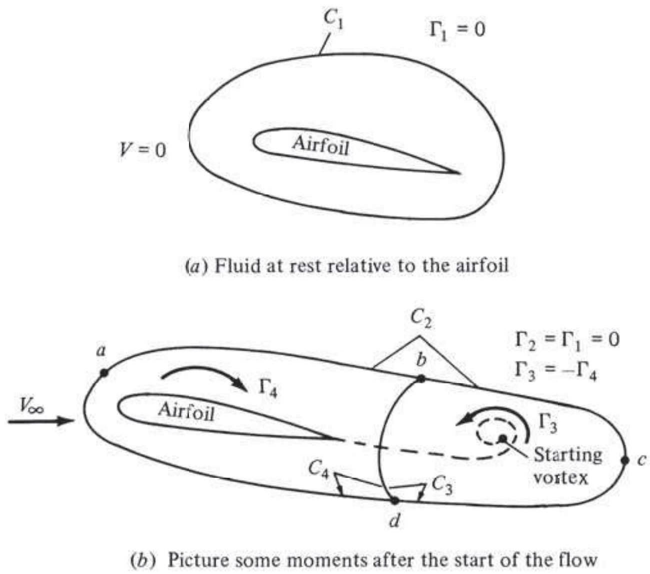

Figure 4.21 The creation of the starting vortex and the resulting generation of circulation around the airfoil.

first principles is left as Problem 4.3. Also, recall our definition and discussion of a vortex sheet in Section 4.4. An interesting consequence of Kelvin's circulation theorem is proof that a stream surface which is a vortex sheet at some instant in time remains a vortex sheet for all times.

Kelvin's theorem helps to explain the generation of circulation around an airfoil, as follows. Consider an airfoil in a fluid at rest, as shown in Figure 4.21*a*. Because $\mathbf{V} = 0$ everywhere, the circulation around curve C_1 is zero. Now start the flow in motion over the airfoil. Initially, the flow will tend to curl around the trailing edge, as explained in Section 4.5 and illustrated at the left of Figure 4.17. In so doing, the velocity at the trailing edge theoretically becomes infinite. In real life, the velocity tends toward a very large finite number. Consequently, during the very first moments after the flow is started, a thin region of very large velocity gradients (and therefore high vorticity) is formed at the trailing edge. This high-vorticity region is fixed to the same fluid elements, and consequently it is flushed downstream as the fluid elements begin to move downstream from the trailing edge. As it moves downstream, this thin sheet of intense vorticity is unstable, and it tends to roll up and form a picture similar to a point vortex. This vortex is called the *starting vortex* and is sketched in Figure 4.21*b*. After the flow around the airfoil has come to a steady state where the flow leaves the trailing edge smoothly (the Kutta condition), the high velocity gradients at the trailing edge disappear and vorticity is no longer produced at that point. However, the starting vortex has already been formed during the starting process, and it moves steadily downstream with the flow forever after. Figure 4.21*b* shows the flow field sometime after steady flow has been achieved over the airfoil, with the starting vortex somewhere downstream. The fluid elements that initially made up curve C_1 in Figure 4.21*a* have moved downstream and now make up curve C_2, which is the complete circuit *abcda* shown in Figure 4.21*b*. Thus, from Kelvin's theorem, the circulation Γ_2 around curve C_2 (which encloses both the airfoil and the starting vortex) is the same as that around curve C_1, namely, zero. $\Gamma_2 = \Gamma_1 = 0$. Now let us subdivide C_2 into two loops by making the cut *bd*, thus forming curves C_3 (circuit *bcdb*) and C_4 (circuit *abda*). Curve C_3 encloses the starting vortex, and curve C_4 encloses the airfoil. The circulation Γ_3 around curve C_3 is due to the starting vortex; by inspecting Figure 4.21*b*, we see that Γ_3 is in the counterclockwise direction (i.e., a negative value). The circulation around curve C_4 enclosing the airfoil is Γ_4. Since the cut *bd* is common to both C_3 and C_4, the sum of the circulations around C_3 and C_4 is simply equal to the circulation around C_2:

$$\Gamma_3 + \Gamma_4 = \Gamma_2$$

However, we have already established that $\Gamma_2 = 0$. Hence,

$$\Gamma_4 = -\Gamma_3$$

that is, the circulation around the airfoil is equal and opposite to the circulation around the starting vortex.

This brings us to the summary as well as the crux of this section. As the flow over an airfoil is started, the large velocity gradients at the sharp trailing edge result in the formation of a region of intense vorticity which rolls up downstream of the trailing edge, forming the starting vortex. This starting vortex has associated with it a counterclockwise circulation. Therefore, as an equal-and-opposite reaction, a clockwise circulation around the airfoil is generated. As the starting process continues, vorticity from the trailing edge is constantly fed into the starting vortex, making it stronger with a consequent larger counterclockwise circulation. In turn, the clockwise circulation around the airfoil becomes stronger, making the flow at the trailing edge more closely approach the Kutta condition, thus weakening the vorticity shed from the trailing edge. Finally, the starting vortex builds up to just the right strength such that the equal-and-opposite clockwise circulation around the airfoil leads to smooth flow from the trailing edge (the Kutta condition is exactly satisfied). When this happens, the vorticity shed from the trailing edge becomes zero, the starting vortex no longer grows in strength, and a steady circulation exists around the airfoil.

EXAMPLE 4.4

For the NACA 2412 airfoil at the conditions given in Example 4.1, calculate the strength of the steady-state starting vortex.

Solution

From the given conditions in Example 4.1,

$$L' = 1254 \text{ N/m}$$

$$V_\infty = 70 \text{ m/s}$$

$$\rho_\infty = 1.23 \text{ kg/m}^3$$

From the Kutta-Joukowski theorem, Equation (3.140),

$$L' = \rho_\infty V_\infty \Gamma$$

the circulation associated with the flow over the airfoil is

$$\Gamma = \frac{L'}{\rho_\infty V_\infty} = \frac{1254}{(1.23)(70)} = 14.56 \ \frac{\text{m}^2}{\text{s}}$$

Referring to Figure 4.21, the steady-state starting vortex has strength equal and opposite to the circulation around the airfoil. Hence,

$$\boxed{\text{Strength of starting vortex} = -14.56 \ \frac{\text{m}^2}{\text{s}}}$$

Note: For practical calculations in aerodynamics, an actual number for circulation is rarely needed. Circulation is a mathematical quantity defined by Equation (2.136), and it is an essential theoretical concept within the framework of the circulation theory of lift. For example, in Section 4.7, an analytical expression for circulation is derived as Equation (4.30), and then immediately inserted into the Kutta-Joukowski theorem, Equation (4.31), yielding a formula for the lift coefficient, Equation (4.33). Nowhere do we need to calculate an actual number for Γ. In the present example, however, the *strength* of the starting vortex is indeed given by its circulation, and hence to compare the strengths of various starting vortices, calculating numbers for Γ is relevant. Even this can be considered only an academic exercise. In this author's experience, no practical aerodynamic calculation requires the strength of a starting vortex. The starting vortex is simply a theoretical construct that is consistent with the generation of circulation around a lifting two-dimensional body.

4.7 CLASSICAL THIN AIRFOIL THEORY: THE SYMMETRIC AIRFOIL

Some experimentally observed characteristics of airfoils and a philosophy for the theoretical prediction of these characteristics have been discussed in the preceding sections. Referring to our chapter road map in Figure 4.7, we have now completed the central branch. In this section, we move to the right-hand branch of Figure 4.7, namely, a quantitative development of thin airfoil theory. The basic equations necessary for the calculation of airfoil lift and moments are established in this section, with an application to symmetric airfoils. The case of cambered airfoils will be treated in Section 4.8.

For the time being, we deal with *thin* airfoils; for such a case, the airfoil can be simulated by a vortex sheet placed along the camber line, as discussed in Section 4.4. Our purpose is to calculate the variation of $\gamma(s)$ such that the camber line becomes a streamline of the flow and such that the Kutta condition is satisfied at the trailing edge; that is, $\gamma(\text{TE}) = 0$ [see Equation (4.10)]. Once we have found the particular $\gamma(s)$ that satisfies these conditions, then the total circulation Γ around the airfoil is found by integrating $\gamma(s)$ from the leading edge to the trailing edge. In turn, the lift is calculated from Γ via the Kutta-Joukowski theorem.

Consider a vortex sheet placed on the camber line of an airfoil, as sketched in Figure 4.22*a*. The freestream velocity is V_∞, and the airfoil is at the angle of attack α. The x axis is oriented along the chord line, and the z axis is perpendicular to the chord. The distance measured along the camber line is denoted by s. The shape of the camber line is given by $z = z(x)$. The chord length is c. In Figure 4.22*a*, w' is the component of velocity normal to the camber line induced by the vortex sheet; $w' = w'(s)$. For a thin airfoil, we rationalized in Section 4.4 that the distribution of a vortex sheet over the surface of the airfoil, when viewed from a distance, looks almost the same as a vortex sheet placed on the camber line. Let us stand back once again and view Figure 4.22*a* from a distance. If the airfoil

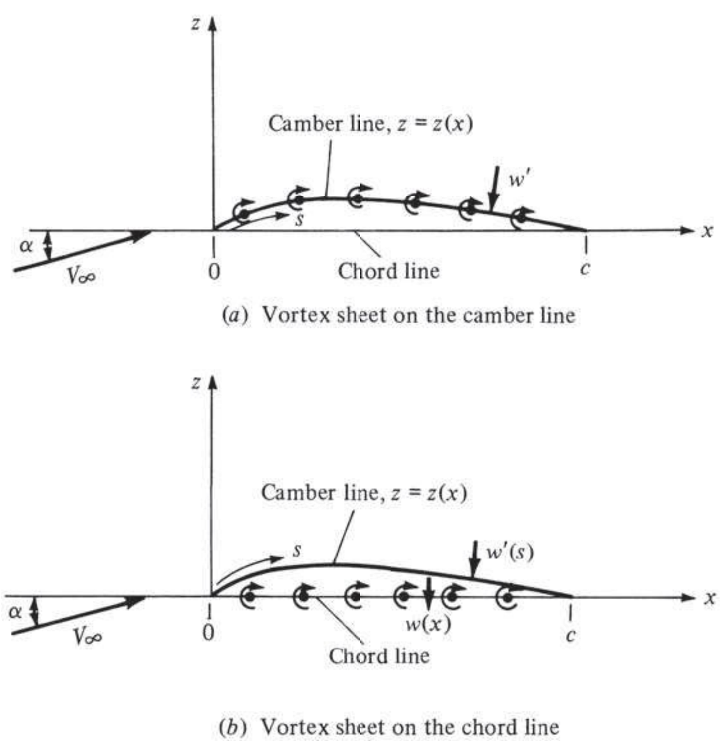

Figure 4.22 Placement of the vortex sheet for thin airfoil analysis.

is thin, the camber line is close to the chord line, and viewed from a distance, the vortex sheet appears to fall approximately on the chord line. Therefore, once again, let us reorient our thinking and place the vortex sheet on the chord line, as sketched in Figure 4.22*b*. Here, $\gamma = \gamma(x)$. We still wish the camber line to be a streamline of the flow, and $\gamma = \gamma(x)$ is calculated to satisfy this condition as well as the Kutta condition $\gamma(c) = 0$. That is, the strength of the vortex sheet on the chord line is determined such that the camber line (not the chord line) is a streamline.

For the camber line to be a streamline, the component of velocity normal to the camber line must be zero at all points along the camber line. The velocity at any point in the flow is the sum of the uniform freestream velocity and the velocity induced by the vortex sheet. Let $V_{\infty,n}$ be the component of the freestream velocity normal to the camber line. Thus, for the camber line to be a streamline,

$$V_{\infty,n} + w'(s) = 0 \tag{4.12}$$

at every point along the camber line.

An expression for $V_{\infty,n}$ in Equation (4.12) is obtained by the inspection of Figure 4.23. At any point P on the camber line, where the slope of the camber line is dz/dx, the geometry of Figure 4.23 yields

$$V_{\infty,n} = V_\infty \sin\left[\alpha + \tan^{-1}\left(-\frac{dz}{dx}\right)\right] \tag{4.13}$$

For a thin airfoil at small angle of attack, both α and $\tan^{-1}(-dz/dx)$ are small values. Using the approximation that $\sin\theta \approx \tan\theta \approx \theta$ for small θ, where θ is in

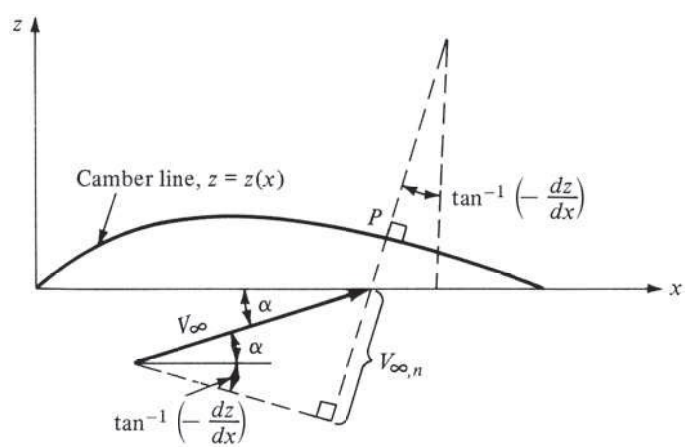

Figure 4.23 Determination of the component of freestream velocity normal to the camber line.

radians, Equation (4.13) reduces to

$$V_{\infty,n} = V_\infty \left(\alpha - \frac{dz}{dx} \right) \tag{4.14}$$

Equation (4.14) gives the expression for $V_{\infty,n}$ to be used in Equation (4.12). Keep in mind that, in Equation (4.14), α is in radians.

Returning to Equation (4.12), let us develop an expression for $w'(s)$ in terms of the strength of the vortex sheet. Refer again to Figure 4.22*b*. Here, the vortex sheet is along the chord line, and $w'(s)$ is the component of velocity normal to the camber line induced by the vortex sheet. Let $w(x)$ denote the component of velocity normal to the *chord line* induced by the vortex sheet, as also shown in Figure 4.22*b*. If the airfoil is thin, the camber line is close to the chord line, and it is consistent with thin airfoil theory to make the approximation that

$$w'(s) \approx w(x) \tag{4.15}$$

An expression for $w(x)$ in terms of the strength of the vortex sheet is easily obtained from Equation (4.1), as follows. Consider Figure 4.24, which shows the vortex sheet along the chord line. We wish to calculate the value of $w(x)$ at the location x. Consider an elemental vortex of strength $\gamma\, d\xi$ located at a distance ξ from the origin along the chord line, as shown in Figure 4.24. The strength of the vortex sheet γ varies with the distance along the chord; that is, $\gamma = \gamma(\xi)$. The velocity dw at point x induced by the elemental vortex at point ξ is given by Equation (4.1) as

$$dw = -\frac{\gamma(\xi)\, d\xi}{2\pi(x - \xi)} \tag{4.16}$$

In turn, the velocity $w(x)$ induced at point x by *all* the elemental vortices along the chord line is obtained by integrating Equation (4.16) from the leading edge ($\xi = 0$) to the trailing edge ($\xi = c$):

$$w(x) = -\int_0^c \frac{\gamma(\xi)\, d\xi}{2\pi(x - \xi)} \tag{4.17}$$

Combined with the approximation stated by Equation (4.15), Equation (4.17) gives the expression for $w'(s)$ to be used in Equation (4.12).

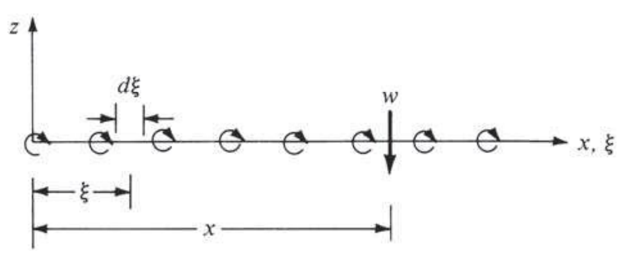

Figure 4.24 Calculation of the induced velocity at the chord line.

Recall that Equation (4.12) is the boundary condition necessary for the camber line to be a streamline. Substituting Equations (4.14), (4.15), and (4.17) into (4.12), we obtain

$$V_\infty\left(\alpha - \frac{dz}{dx}\right) - \int_0^c \frac{\gamma(\xi)\,d\xi}{2\pi(x-\xi)} = 0$$

or

$$\boxed{\frac{1}{2\pi}\int_0^c \frac{\gamma(\xi)\,d\xi}{x-\xi} = V_\infty\left(\alpha - \frac{dz}{dx}\right)} \tag{4.18}$$

the *fundamental equation of thin airfoil theory;* it is simply a statement that the camber line is a streamline of the flow.

Note that Equation (4.18) is written at a given point x on the chord line, and that dz/dx is evaluated at that point x. The variable ξ is simply a dummy variable of integration which varies from 0 to c along the chord line, as shown in Figure 4.24. The vortex strength $\gamma = \gamma(\xi)$ is a variable along the chord line. For a given airfoil at a given angle of attack, both α and dz/dx are known values in Equation (4.18). Indeed, the only unknown in Equation (4.18) is the vortex strength $\gamma(\xi)$. Hence, Equation (4.18) is an integral equation, the solution of which yields the variation of $\gamma(\xi)$ such that the camber line is a streamline of the flow. The central problem of thin airfoil theory is to solve Equation (4.18) for $\gamma(\xi)$, subject to the Kutta condition, namely, $\gamma(c) = 0$.

In this section, we treat the case of a symmetric airfoil. As stated in Section 4.2, a symmetric airfoil has no camber; the camber line is coincident with the chord line. Hence, for this case, $dz/dx = 0$, and Equation (4.18) becomes

$$\frac{1}{2\pi}\int_0^c \frac{\gamma(\xi)\,d\xi}{x-\xi} = V_\infty\alpha \tag{4.19}$$

In essence, within the framework of thin airfoil theory, a symmetric airfoil is treated the same as a flat plate; note that our theoretical development does not account for the airfoil thickness distribution. Equation (4.19) is an *exact* expression for the inviscid, incompressible flow over a flat plate at a small angle of attack.

To help deal with the integral in Equations (4.18) and (4.19), let us transform ξ into θ via the following transformation:

$$\xi = \frac{c}{2}(1-\cos\theta) \tag{4.20}$$

Since x is a fixed point in Equations (4.18) and (4.19), it corresponds to a particular value of θ, namely, θ_0, such that

$$x = \frac{c}{2}(1-\cos\theta_0) \tag{4.21}$$

Also, from Equation (4.20),

$$d\xi = \frac{c}{2}\sin\theta\,d\theta \tag{4.22}$$

Substituting Equations (4.20) to (4.22) into (4.19), and noting that the limits of integration become $\theta = 0$ at the leading edge (where $\xi = 0$) and $\theta = \pi$ at the trailing edge (where $\xi = c$), we obtain

$$\frac{1}{2\pi}\int_0^\pi \frac{\gamma(\theta)\sin\theta\, d\theta}{\cos\theta - \cos\theta_0} = V_\infty \alpha \tag{4.23}$$

A rigorous solution of Equation (4.23) for $\gamma(\theta)$ can be obtained from the mathematical theory of integral equations, which is beyond the scope of this book. Instead, we simply state that the solution is

$$\boxed{\gamma(\theta) = 2\alpha V_\infty \frac{(1+\cos\theta)}{\sin\theta}} \tag{4.24}$$

We can verify this solution by substituting Equation (4.24) into (4.23) yielding

$$\frac{1}{2\pi}\int_0^\pi \frac{\gamma(\theta)\sin\theta\, d\theta}{\cos\theta - \cos\theta_0} = \frac{V_\infty \alpha}{\pi}\int_0^\pi \frac{(1+\cos\theta)\, d\theta}{\cos\theta - \cos\theta_0} \tag{4.25}$$

The following standard integral appears frequently in airfoil theory and is derived in Appendix E of Reference 9:

$$\int_0^\pi \frac{\cos n\theta\, d\theta}{\cos\theta - \cos\theta_0} = \frac{\pi \sin n\theta_0}{\sin\theta_0} \tag{4.26}$$

Using Equation (4.26) in the right-hand side of Equation (4.25), we find that

$$\frac{V_\infty \alpha}{\pi}\int_0^\pi \frac{(1+\cos\theta)\, d\theta}{\cos\theta - \cos\theta_0} = \frac{V_\infty \alpha}{\pi}\left(\int_0^\pi \frac{d\theta}{\cos\theta - \cos\theta_0} + \int_0^\pi \frac{\cos\theta\, d\theta}{\cos\theta - \cos\theta_0}\right)$$

$$= \frac{V_\infty \alpha}{\pi}(0 + \pi) = V_\infty \alpha \tag{4.27}$$

Substituting Equation (4.27) into (4.25), we have

$$\frac{1}{2\pi}\int_0^\pi \frac{\gamma(\theta)\sin\theta\, d\theta}{\cos\theta - \cos\theta_0} = V_\infty \alpha$$

which is identical to Equation (4.23). Hence, we have shown that Equation (4.24) is indeed the solution to Equation (4.23). Also, note that at the trailing edge, where $\theta = \pi$, Equation (4.24) yields

$$\gamma(\pi) = 2\alpha V_\infty \frac{0}{0}$$

which is an indeterminant form. However, using L'Hospital's rule on Equation (4.24),

$$\gamma(\pi) = 2\alpha V_\infty \frac{-\sin\pi}{\cos\pi} = 0$$

Thus, Equation (4.24) also satisfies the Kutta condition.

We are now in a position to calculate the lift coefficient for a thin, symmetric airfoil. The total circulation around the airfoil is

$$\Gamma = \int_0^c \gamma(\xi)\, d\xi \tag{4.28}$$

Using Equations (4.20) and (4.22), Equation (4.28) transforms to

$$\Gamma = \frac{c}{2}\int_0^\pi \gamma(\theta)\sin\theta\, d\theta \tag{4.29}$$

Substituting Equation (4.24) into (4.29), we obtain

$$\Gamma = \alpha c V_\infty \int_0^\pi (1+\cos\theta)\, d\theta = \pi\alpha c V_\infty \tag{4.30}$$

Substituting Equation (4.30) into the Kutta-Joukowski theorem, we find that the lift per unit span is

$$L' = \rho_\infty V_\infty \Gamma = \pi\alpha c\rho_\infty V_\infty^2 \tag{4.31}$$

The lift coefficient is

$$c_l = \frac{L'}{q_\infty S} \tag{4.32}$$

where $$S = c(1)$$

Substituting Equation (4.31) into (4.32), we have

$$c_l = \frac{\pi\alpha c\rho_\infty V_\infty^2}{\frac{1}{2}\rho_\infty V_\infty^2 c(1)}$$

or $$\boxed{c_l = 2\pi\alpha} \tag{4.33}$$

and $$\boxed{\text{Lift slope} = \frac{dc_l}{d\alpha} = 2\pi} \tag{4.34}$$

Equations (4.33) and (4.34) are important results; they state the theoretical result that the lift coefficient is *linearly proportional to angle of attack,* which is supported by the experimental results discussed in Section 4.3. They also state that the theoretical lift slope is equal to 2π rad^{-1}, which is 0.11 degree^{-1}. The experimental lift coefficient data for an NACA 0012 symmetric airfoil are given in Figure 4.25; note that Equation (4.33) accurately predicts c_l over a large range of angle of attack. (The NACA 0012 airfoil section is commonly used on airplane tails and helicopter blades.)

The moment about the leading edge can be calculated as follows. Consider the elemental vortex of strength $\gamma(\xi)\, d\xi$ located a distance ξ from the leading edge, as sketched in Figure 4.26. The circulation associated with this elemental vortex is $d\Gamma = \gamma(\xi)\, d\xi$. In turn, the increment of lift dL contributed by the elemental vortex is $dL = \rho_\infty V_\infty\, d\Gamma$. This increment of lift creates a moment about the leading edge $dM = -\xi(dL)$. The total moment about the leading edge

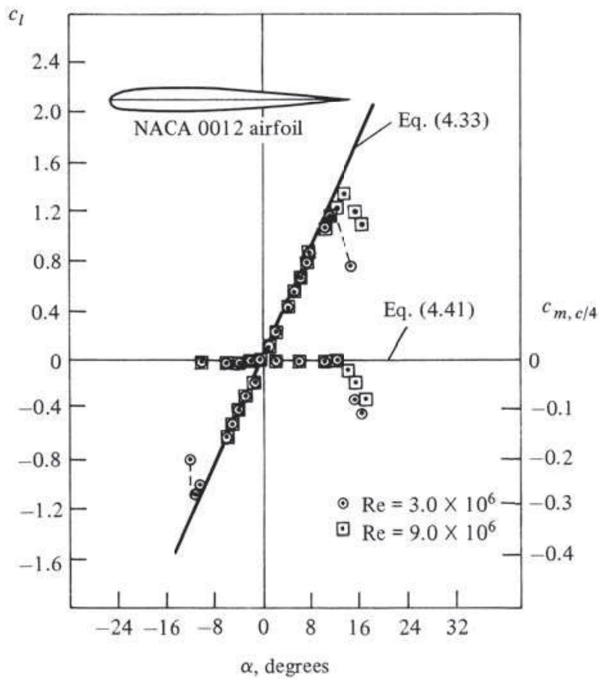

Figure 4.25 Comparison between theory and experiment for the lift and moment coefficients for an NACA 0012 airfoil. (Data Source: Abbott, I. H., and A. E. von Doenhoff: *Theory of Wing Sections*, McGraw-Hill Book Company, New York, 1949; also, Dover Publications, Inc., New York, 1959.)

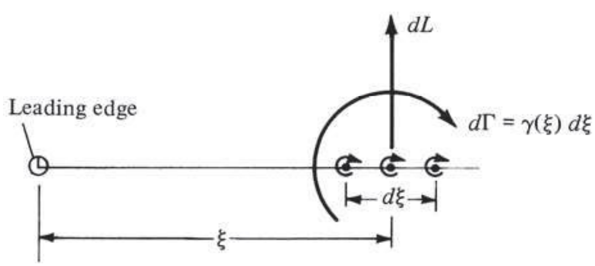

Figure 4.26 Calculation of moments about the leading edge.

(LE) (per unit span) due to the entire vortex sheet is therefore

$$M'_{\text{LE}} = -\int_0^c \xi(dL) = -\rho_\infty V_\infty \int_0^c \xi\gamma(\xi)\,d\xi \tag{4.35}$$

Transforming Equation (4.35) via Equations (4.20) and (4.22), and performing the integration, we obtain (the details are left for Problem 4.4):

$$M'_{\text{LE}} = -q_\infty c^2 \frac{\pi\alpha}{2} \tag{4.36}$$

The moment coefficient is

$$c_{m,\text{le}} = \frac{M'_{\text{LE}}}{q_\infty S c}$$

where $S = c(1)$. Hence,

$$c_{m,\text{le}} = \frac{M'_{\text{LE}}}{q_\infty c^2} = -\frac{\pi\alpha}{2} \tag{4.37}$$

However, from Equation (4.33),

$$\pi\alpha = \frac{c_l}{2} \tag{4.38}$$

Combining Equations (4.37) and (4.38), we obtain

$$\boxed{c_{m,\text{le}} = -\frac{c_l}{4}} \tag{4.39}$$

From Equation (1.22), the moment coefficient about the quarter-chord point is

$$c_{m,c/4} = c_{m,\text{le}} + \frac{c_l}{4} \tag{4.40}$$

Combining Equations (4.39) and (4.40), we have

$$\boxed{c_{m,c/4} = 0} \tag{4.41}$$

In Section 1.6, a definition is given for the center of pressure as that point about which the moments are zero. Clearly, Equation (4.41) demonstrates the theoretical result that the *center of pressure is at the quarter-chord point for a symmetric airfoil*.

By the definition given in Section 4.3, that point on an airfoil where moments are independent of angle of attack is called the aerodynamic center. From Equation (4.41), the moment about the quarter chord is zero for all values of α. Hence, for a symmetric airfoil, we have the theoretical result that the *quarter-chord point is both the center of pressure and the aerodynamic center*.

The theoretical result for $c_{m,c/4} = 0$ in Equation (4.41) is supported by the experimental data given in Figure 4.25. Also, note that the experimental value of $c_{m,c/4}$ is constant over a wide range of α, thus demonstrating that the real aerodynamic center is essentially at the quarter chord.

Let us summarize the above results. The essence of thin airfoil theory is to find a distribution of vortex sheet strength along the chord line that will make the camber line a streamline of the flow while satisfying the Kutta condition $\gamma(\text{TE}) = 0$. Such a vortex distribution is obtained by solving Equation (4.18) for $\gamma(\xi)$, or in terms of the transformed independent variable θ, solving Equation (4.23) for $\gamma(\theta)$ [recall that Equation (4.23) is written for a symmetric airfoil]. The resulting vortex distribution $\gamma(\theta)$ for a symmetric airfoil is given by Equation (4.24). In turn, this vortex distribution, when inserted into the Kutta-Joukowski theorem, gives the following important theoretical results for a symmetric airfoil:

1. $c_l = 2\pi\alpha$.
2. Lift slope $= 2\pi$.
3. The center of pressure and the aerodynamic center are both located at the quarter-chord point.

EXAMPLE 4.5

Consider a thin flat plate at 5 deg. angle of attack. Calculate the: (*a*) lift coefficient, (*b*) moment coefficient about the leading edge, (*c*) moment coefficient about the quarter-chord point, and (*d*) moment coefficient about the trailing edge.

Solution

Recall that the results obtained in Section 4.7, although couched in terms of a thin symmetric airfoil, apply in particular to a flat plate with zero thickness.

(*a*) From Equation (4.33),

$$c_\ell = 2\pi\alpha$$

where α is in radians

$$\alpha = \frac{5}{57.3} = 0.0873 \text{ rad}$$

$$c_\ell = 2\pi(0.0873) = \boxed{0.5485}$$

(*b*) From Equation (4.39),

$$c_{m,\ell e} = -\frac{c_\ell}{4} = -\frac{0.5485}{4} = \boxed{-0.137}$$

(*c*) From Equation (4.41),

$$c_{m,c/4} = \boxed{0}$$

(*d*) Figure 4.27 is a sketch of the force and moment system on the plate. We place the lift at the quarter-chord point, along with the moment about the quarter-chord point.

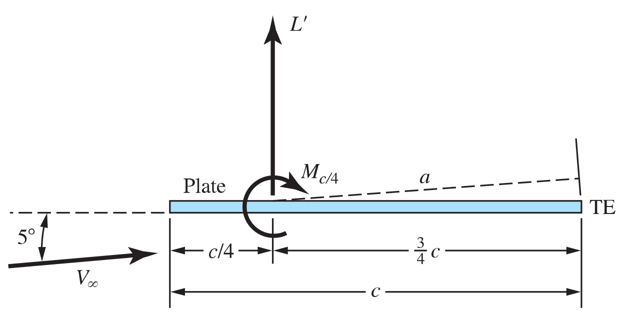

Figure 4.27 Flat plate at 5-degree angle of attack.

This represents the force and moment system on the plate. Recall from the discussion in Section 1.6 that the force and moment system can be represented by the lift acting through any point on the plate, and giving the moment about that point. Here, for convenience, we place the lift at the quarter-chord point.

The lift acts perpendicular to V_∞. [Part of the statement of the Kutta-Joukowski theorem given by Equation (3.140) is that the direction of the force associated with the circulation Γ is perpendicular to V_∞.] From Figure 4.27, the moment arm from L' to the trailing edge is the length a, where

$$a = \left(\tfrac{3}{4}c\right)\cos\alpha = \left(\tfrac{3}{4}c\right)\cos 5^\circ$$

One of the assumptions of thin airfoil theory is that the angle of attack is small, and hence we can assume that $\cos\alpha \approx 1$. Therefore, the moment arm from the point of action of the lift to the trailing edge is reasonably given by $\frac{3}{4}c$. (Note that, in the previous Figure 4.26, the assumption of small α is already implicit because the moment arm is drawn parallel to the plate.)

Examining Figure 4.27, the moment about the trailing edge is

$$M'_{\text{te}} = \left(\frac{3}{4}c\right)L' + M'_{c/4}$$

$$c_{m,\text{te}} = \frac{M'_{\text{te}}}{q_\infty c^2} = \left(\frac{3}{4}c\right)\frac{L'}{q_\infty c^2} + \frac{M'_{c/4}}{q_\infty c^2}$$

$$c_{m,\text{te}} = \frac{3}{4}c_\ell + c_{m,c/4}$$

Since $c_{m,c/4} = 0$ we have

$$c_{m,\text{te}} = \frac{3}{4}c_\ell$$

$$c_{m,\text{te}} = \frac{3}{4}(0.5485) = \boxed{0.411}$$

4.8 THE CAMBERED AIRFOIL

Thin airfoil theory for a cambered airfoil is a generalization of the method for a symmetric airfoil discussed in Section 4.7. To treat the cambered airfoil, return to Equation (4.18):

$$\frac{1}{2\pi}\int_0^c \frac{\gamma(\xi)\,d\xi}{x-\xi} = V_\infty\left(\alpha - \frac{dz}{dx}\right) \tag{4.18}$$

For a cambered airfoil, dz/dx is finite, and this makes the analysis more elaborate than in the case of a symmetric airfoil, where $dz/dx = 0$. Once again, let us transform Equation (4.18) via Equations (4.20) to (4.22), obtaining

$$\frac{1}{2\pi}\int_0^\pi \frac{\gamma(\theta)\sin\theta\,d\theta}{\cos\theta - \cos\theta_0} = V_\infty\left(\alpha - \frac{dz}{dx}\right) \tag{4.42}$$

We wish to obtain a solution for $\gamma(\theta)$ from Equation (4.42), subject to the Kutta condition $\gamma(\pi) = 0$. Such a solution for $\gamma(\theta)$ will make the camber line a streamline of the flow. However, as before a rigorous solution of Equation (4.42) for $\gamma(\theta)$ is beyond the scope of this book. Rather, the result is stated below:

$$\gamma(\theta) = 2V_\infty \left(A_0 \frac{1+\cos\theta}{\sin\theta} + \sum_{n=1}^{\infty} A_n \sin n\theta \right) \tag{4.43}$$

Note that the above expression for $\gamma(\theta)$ consists of a leading term very similar to Equation (4.24) for a symmetric airfoil, plus a Fourier sine series with coefficients A_n. The values of A_n depend on the shape of the camber line dz/dx, and A_0 depends on both dz/dx and α, as shown below.

The coefficients A_0 and $A_n (n = 1, 2, 3, \ldots)$ in Equation (4.43) must be specific values in order that the camber line be a streamline of the flow. To find these specific values, substitute Equations (4.43) into Equation (4.42):

$$\frac{1}{\pi}\int_0^\pi \frac{A_0(1+\cos\theta)\,d\theta}{\cos\theta - \cos\theta_0} + \frac{1}{\pi}\sum_{n=1}^{\infty}\int_0^\pi \frac{A_n \sin n\theta \sin\theta\, d\theta}{\cos\theta - \cos\theta_0} = \alpha - \frac{dz}{dx} \tag{4.44}$$

The first integral can be evaluated from the standard form given in Equation (4.26). The remaining integrals can be obtained from another standard form, which is derived in Appendix E of Reference 9, and which is given below:

$$\int_0^\pi \frac{\sin n\theta \sin\theta\, d\theta}{\cos\theta - \cos\theta_0} = -\pi \cos n\theta_0 \tag{4.45}$$

Hence, using Equations (4.26) and (4.45), we can reduce Equation (4.44) to

$$A_0 - \sum_{n=1}^{\infty} A_n \cos n\theta_0 = \alpha - \frac{dz}{dx}$$

or

$$\frac{dz}{dx} = (\alpha - A_0) + \sum_{n=1}^{\infty} A_n \cos n\theta_0 \tag{4.46}$$

Recall that Equation (4.46) was obtained directly from Equation (4.42), which is the transformed version of the fundamental equation of thin airfoil theory, Equation (4.18). Furthermore, recall that Equation (4.18) is evaluated at a given point x along the chord line, as sketched in Figure 4.24. Hence, Equation (4.46) is also evaluated at the given point x; here, dz/dx and θ_0 correspond to the same point x on the chord line. Also, recall that dz/dx is a function of θ_0, where $x = (c/2)(1 - \cos\theta_0)$ from Equation (4.21).

Examine Equation (4.46) closely. It is in the form of a Fourier cosine series expansion for the function of dz/dx. In general, the Fourier cosine series representation of a function $f(\theta)$ over an interval $0 \le \theta \le \pi$ is given by

$$f(\theta) = B_0 + \sum_{n=1}^{\infty} B_n \cos n\theta \tag{4.47}$$

where, from Fourier analysis, the coefficients B_0 and B_n are given by

$$B_0 = \frac{1}{\pi} \int_0^\pi f(\theta)\, d\theta \tag{4.48}$$

and

$$B_n = \frac{2}{\pi} \int_0^\pi f(\theta) \cos n\theta \, d\theta \tag{4.49}$$

(See, e.g., page 217 of Reference 6.) In Equation (4.46), the function dz/dx is analogous to $f(\theta)$ in the general form given in Equation (4.47). Thus, from Equations (4.48) and (4.49), the coefficients in Equation (4.46) are given by

$$\alpha - A_0 = \frac{1}{\pi} \int_0^\pi \frac{dz}{dx}\, d\theta_0$$

or

$$A_0 = \alpha - \frac{1}{\pi} \int_0^\pi \frac{dz}{dx}\, d\theta_0 \tag{4.50}$$

and

$$A_n = \frac{2}{\pi} \int_0^\pi \frac{dz}{dx} \cos n\theta_0 \, d\theta_0 \tag{4.51}$$

Keep in mind that in the above, dz/dx is a function of θ_0. Note from Equation (4.50) that A_0 depends on both α and the shape of the camber line (through dz/dx), whereas from Equation (4.51) the values of A_n depend only on the shape of the camber line.

Pause for a moment and think about what we have done. We are considering the flow over a cambered airfoil of given shape dz/dx at a given angle of attack α. In order to make the camber line a streamline of the flow, the strength of the vortex sheet along the chord line must have the distribution $\gamma(\theta)$ given by Equation (4.43), where the coefficients A_0 and A_n are given by Equations (4.50) and (4.51), respectively. Also, note that Equation (4.43) satisfies the Kutta condition $\gamma(\pi) = 0$. Actual numbers for A_0 and A_n can be obtained for a given shape airfoil at a given angle of attack simply by carrying out the integrations indicated in Equations (4.50) and (4.51). For an example of such calculations applied to an NACA 23012 airfoil, see Example 4.5 at the end of this section. Also, note that when $dz/dx = 0$, Equation (4.43) reduces to Equation (4.24) for a symmetric airfoil. Hence, the symmetric airfoil is a special case of Equation (4.43).

Let us now obtain expressions for the aerodynamic coefficients for a cambered airfoil. The total circulation due to the entire vortex sheet from the leading edge to the trailing edge is

$$\Gamma = \int_0^c \gamma(\xi)\, d\xi = \frac{c}{2} \int_0^\pi \gamma(\theta) \sin\theta \, d\theta \tag{4.52}$$

Substituting Equation (4.43) for $\gamma(\theta)$ into Equation (4.52), we obtain

$$\Gamma = cV_\infty \left[A_0 \int_0^\pi (1 + \cos\theta)\, d\theta + \sum_{n=1}^{\infty} A_n \int_0^\pi \sin n\theta \sin\theta \, d\theta \right] \tag{4.53}$$

From any standard table of integrals,

$$\int_0^{\pi} (1 + \cos\theta)\, d\theta = \pi$$

and
$$\int_0^{\pi} \sin n\theta \sin\theta\, d\theta = \begin{cases} \pi/2 & \text{for } n = 1 \\ 0 & \text{for } n \neq 1 \end{cases}$$

Hence, Equation (4.53) becomes

$$\Gamma = cV_\infty \left(\pi A_0 + \frac{\pi}{2} A_1\right) \tag{4.54}$$

From Equation (4.54), the lift per unit span is

$$L' = \rho_\infty V_\infty \Gamma = \rho_\infty V_\infty^2 c \left(\pi A_0 + \frac{\pi}{2} A_1\right) \tag{4.55}$$

In turn, Equation (4.55) leads to the lift coefficient in the form

$$c_l = \frac{L'}{\frac{1}{2}\rho_\infty V_\infty^2 c(1)} = \pi(2A_0 + A_1) \tag{4.56}$$

Recall that the coefficients A_0 and A_1 in Equation (4.56) are given by Equations (4.50) and (4.51), respectively. Hence, Equation (4.56) becomes

$$\boxed{c_l = 2\pi \left[\alpha + \frac{1}{\pi}\int_0^{\pi} \frac{dz}{dx}(\cos\theta_0 - 1)\, d\theta_0\right]} \tag{4.57}$$

and
$$\boxed{\text{Lift slope} \equiv \frac{dc_l}{d\alpha} = 2\pi} \tag{4.58}$$

Equations (4.57) and (4.58) are important results. Note that, as in the case of the symmetric airfoil, the theoretical lift slope for a cambered airfoil is 2π. It is a general result from thin airfoil theory that $dc_l/d\alpha = 2\pi$ for any shape airfoil. However, the expression for c_l itself differs between a symmetric and a cambered airfoil, the difference being the integral term in Equation (4.57). This integral term has physical significance, as follows. Return to Figure 4.9, which illustrates the lift curve for an airfoil. The angle of zero lift is denoted by $\alpha_{L=0}$ and is a negative value. From the geometry shown in Figure 4.9, clearly

$$c_l = \frac{dc_l}{d\alpha}(\alpha - \alpha_{L=0}) \tag{4.59}$$

Substituting Equation (4.58) into (4.59), we have

$$c_l = 2\pi(\alpha - \alpha_{L=0}) \tag{4.60}$$

Comparing Equations (4.60) and (4.57), we see that the integral term in Equation (4.57) is simply the negative of the zero-lift angle; that is,

$$\boxed{\alpha_{L=0} = -\frac{1}{\pi}\int_0^{\pi} \frac{dz}{dx}(\cos\theta_0 - 1)\, d\theta_0} \tag{4.61}$$

Hence, from Equation (4.61), thin airfoil theory provides a means to predict the angle of zero lift. Note that Equation (4.61) yields $\alpha_{L=0} = 0$ for a symmetric airfoil, which is consistent with the results shown in Figure 4.25. Also, note that the more highly cambered the airfoil, the larger will be the absolute magnitude of $\alpha_{L=0}$.

Returning to Figure 4.26, the moment about the leading edge can be obtained by substituting $\gamma(\theta)$ from Equation (4.43) into the transformed version of Equation (4.35). The details are left for Problem 4.9. The result for the moment coefficient is

$$c_{m,\text{le}} = -\frac{\pi}{2}\left(A_0 + A_1 - \frac{A_2}{2}\right) \tag{4.62}$$

Substituting Equation (4.56) into (4.62), we have

$$\boxed{c_{m,\text{le}} = -\left[\frac{c_l}{4} + \frac{\pi}{4}(A_1 - A_2)\right]} \tag{4.63}$$

Note that, for $dz/dx = 0$, $A_1 = A_2 = 0$ and Equation (4.63) reduces to Equation (4.39) for a symmetric airfoil.

The moment coefficient about the quarter chord can be obtained by substituting Equation (4.63) into (4.40), yielding

$$\boxed{c_{m,c/4} = \frac{\pi}{4}(A_2 - A_1)} \tag{4.64}$$

Unlike the symmetric airfoil, where $c_{m,c/4} = 0$, Equation (4.64) demonstrates that $c_{m,c/4}$ is finite for a cambered airfoil. Therefore, the quarter chord is *not* the center of pressure for a cambered airfoil. However, note that A_1 and A_2 depend only on the shape of the camber line and do not involve the angle of attack. Hence, from Equation (4.64), $c_{m,c/4}$ is *independent* of α. Thus, the quarter-chord point is the *theoretical location* of the aerodynamic center for a cambered airfoil.

The location of the center of pressure can be obtained from Equation (1.21):

$$x_{\text{cp}} = -\frac{M'_{\text{LE}}}{L'} = -\frac{c_{m,\text{le}}c}{c_l} \tag{4.65}$$

Substituting Equation (4.63) into (4.65), we obtain

$$\boxed{x_{\text{cp}} = \frac{c}{4}\left[1 + \frac{\pi}{c_l}(A_1 - A_2)\right]} \tag{4.66}$$

Equation (4.66) demonstrates that the center of pressure for a cambered airfoil varies with the lift coefficient. Hence, as the angle of attack changes, the center of pressure also changes. Indeed, as the lift approaches zero, x_{cp} moves toward infinity; that is, it leaves the airfoil. For this reason, the center of pressure is not always a convenient point at which to draw the force system on an airfoil. Rather, the force-and-moment system on an airfoil is more conveniently considered at the aerodynamic center. (Return to Figure 1.25 and the discussion at the end of Section 1.6 for the referencing of the force-and-moment system on an airfoil.)

EXAMPLE 4.6

Consider an NACA 23012 airfoil. The mean camber line for this airfoil is given by

$$\frac{z}{c} = 2.6595\left[\left(\frac{x}{c}\right)^3 - 0.6075\left(\frac{x}{c}\right)^2 + 0.1147\left(\frac{x}{c}\right)\right] \qquad \text{for } 0 \le \frac{x}{c} \le 0.2025$$

and
$$\frac{z}{c} = 0.02208\left(1 - \frac{x}{c}\right) \qquad \text{for } 0.2025 \le \frac{x}{c} \le 1.0$$

Calculate (*a*) the angle of attack at zero lift, (*b*) the lift coefficient when $\alpha = 4^\circ$, (*c*) the moment coefficient about the quarter chord, and (*d*) the location of the center of pressure in terms of x_{cp}/c, when $\alpha = 4^\circ$. Compare the results with experimental data.

Solution

We will need dz/dx. From the given shape of the mean camber line, this is

$$\frac{dz}{dx} = 2.6595\left[3\left(\frac{x}{c}\right)^2 - 1.215\left(\frac{x}{c}\right) + 0.1147\right] \qquad \text{for } 0 \le \frac{x}{c} \le 0.2025$$

and
$$\frac{dz}{dx} = -0.02208 \qquad \text{for } 0.2025 \le \frac{x}{c} \le 1.0$$

Transforming from x to θ, where $x = (c/2)(1 - \cos\theta)$, we have

$$\frac{dz}{dx} = 2.6595\left[\frac{3}{4}(1 - 2\cos\theta + \cos^2\theta) - 0.6075(1 - \cos\theta) + 0.1147\right]$$

or
$$= 0.6840 - 2.3736\cos\theta + 1.995\cos^2\theta \qquad \text{for } 0 \le \theta \le 0.9335 \text{ rad}$$

and
$$= -0.02208 \qquad \text{for } 0.9335 \le \theta \le \pi$$

(*a*) From Equation (4.61),

$$\alpha_{L=0} = -\frac{1}{\pi}\int_0^\pi \frac{dz}{dx}(\cos\theta - 1)\, d\theta$$

(*Note:* For simplicity, we have dropped the subscript zero from θ; in Equation (4.61), θ_0 is the variable of integration—it can just as well be symbolized as θ for the variable of integration.) Substituting the equation for dz/dx into Equation (4.61), we have

$$\alpha_{L=0} = -\frac{1}{\pi}\int_0^{0.9335} (-0.6840 + 3.0576\cos\theta - 4.3686\cos^2\theta + 1.995\cos^3\theta)\, d\theta$$
$$-\frac{1}{\pi}\int_{0.9335}^{\pi} (0.02208 - 0.02208\cos\theta)\, d\theta \qquad \text{(E.1)}$$

From a table of integrals, we see that

$$\int \cos\theta\, d\theta = \sin\theta$$

$$\int \cos^2\theta\, d\theta = \tfrac{1}{2}\sin\theta\cos\theta + \tfrac{1}{2}\theta$$

$$\int \cos^3\theta\, d\theta = \tfrac{1}{3}\sin\theta(\cos^2\theta + 2)$$

Hence, Equation (E.1) becomes

$$\begin{aligned}\alpha_{L=0} = &-\frac{1}{\pi}[-2.8683\theta + 3.0576\sin\theta - 2.1843\sin\theta\cos\theta \\ &+ 0.665\sin\theta(\cos^2\theta + 2)]_0^{0.9335} \\ &-\frac{1}{\pi}[0.022208\theta - 0.02208\sin\theta]_{0.9335}^{\pi}\end{aligned}$$

Hence, $$\alpha_{L=0} = -\frac{1}{\pi}(-0.0065 + 0.0665) = -0.0191 \text{ rad}$$

or $$\boxed{\alpha_{L=0} = -1.09^\circ}$$

(*b*) $\alpha = 4^\circ = 0.0698$ rad
From Equation (4.60),

$$c_l = 2\pi(\alpha - \alpha_{L=0}) = 2\pi(0.0698 + 0.0191) = \boxed{0.559}$$

(*c*) The value of $c_{m,c/4}$ is obtained from Equation (4.64). For this, we need the two Fourier coefficients A_1 and A_2. From Equation (4.51),

$$A_1 = \frac{2}{\pi}\int_0^{\pi} \frac{dz}{dx}\cos\theta\, d\theta$$

$$\begin{aligned}A_1 &= \frac{2}{\pi}\int_0^{0.9335}(0.6840\cos\theta - 2.3736\cos^2\theta + 1.995\cos^3\theta)\, d\theta \\ &\quad + \frac{2}{\pi}\int_{0.9335}^{\pi}(-0.02208\cos\theta)\, d\theta \\ &= \frac{2}{\pi}[0.6840\sin\theta - 1.1868\sin\theta\cos\theta - 1.1868\theta + 0.665\sin\theta(\cos^2\theta + 2)]_0^{0.9335} \\ &\quad + \frac{2}{\pi}[-0.02208\sin\theta]_{0.09335}^{\pi} \\ &= \frac{2}{\pi}(0.1322 + 0.0177) = 0.0954\end{aligned}$$

From Equation (4.51),

$$A_2 = \frac{2}{\pi}\int_0^{\pi} \frac{dz}{dx}\cos 2\theta \, d\theta = \frac{2}{\pi}\int_0^{\pi} \frac{dz}{dx}(2\cos^2\theta - 1)\, d\theta$$

$$= \frac{2}{\pi}\int_0^{0.9335} (-0.6840 + 2.3736\cos\theta - 0.627\cos^2\theta$$

$$- 4.747\cos^3\theta + 3.99\cos^4\theta)\, d\theta$$

$$+ \frac{2}{\pi}\int_{0.9335}^{\pi} (0.02208 - 0.0446\cos^2\theta)\, d\theta$$

Note:

$$\int \cos^4\theta \, d\theta = \tfrac{1}{4}\cos^3\theta\sin\theta + \tfrac{3}{8}(\sin\theta\cos\theta + \theta)$$

Thus,

$$A_2 = \frac{2}{\pi}\left\{-0.6840\,\theta + 2.3736\sin\theta - 0.628\left(\frac{1}{2}\right)(\sin\theta\cos\theta + \theta)\right.$$

$$\left. - 4.747\left(\frac{1}{3}\right)\sin\theta(\cos^2\theta + 2) + 3.99\left[\frac{1}{4}\cos^3\sin\theta + \frac{3}{8}(\sin\theta\cos\theta + \theta)\right]\right\}_0^{0.9335}$$

$$+ \frac{2}{\pi}\left[0.02208\theta - 0.0446\left(\frac{1}{2}\right)(\sin\theta\cos\theta + \theta)\right]_{0.9335}^{\pi}$$

$$= \frac{2}{\pi}(0.11384 + 0.01056) = 0.0792$$

From Equation (4.64),

$$c_{m,c/4} = \frac{\pi}{4}(A_2 - A_1) = \frac{\pi}{4}(0.0792 - 0.0954)$$

$$\boxed{c_{m,c/4} = -0.0127}$$

(*d*) From Equation (4.66),

$$x_{\text{cp}} = \frac{c}{4}\left[1 + \frac{\pi}{c_l}(A_1 - A_2)\right]$$

Hence,
$$\frac{x_{\text{cp}}}{c} = \frac{1}{4}\left[1 + \frac{\pi}{0.559}(0.0954 - 0.0792)\right] = 0.273$$

Comparison with Experimental Data The data for the NACA 23012 airfoil are shown in Figure 4.28. From this, we make the following tabulation:

	Calculated	Experiment
$\alpha_{L=0}$	$-1.09°$	$-1.1°$
c_l (at $\alpha = 4°$)	0.559	0.55
$c_{m,c/4}$	-0.0127	-0.01

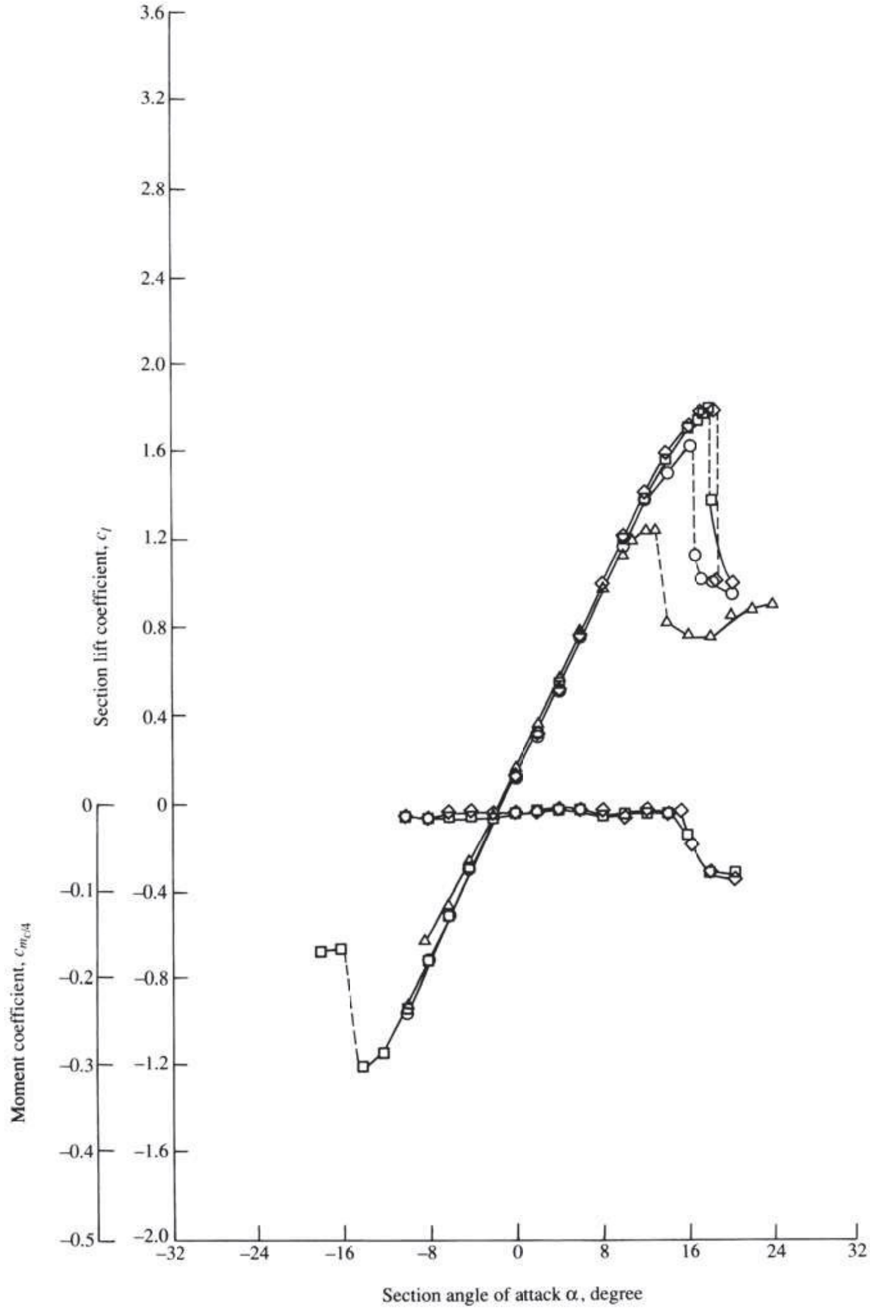

Figure 4.28 Lift- and moment-coefficient data for an NACA 23012 airfoil, for comparison with the theoretical results obtained in Example 4.6.

Note that the results from thin airfoil theory for a cambered airfoil agree very well with the experimental data. Recall that excellent agreement between thin airfoil theory for a symmetric airfoil and experimental data has already been shown in Figure 4.25. Hence, all of the work we have done in this section to develop thin airfoil theory is certainly worth the effort. Moreover, this illustrates that the development of thin airfoil theory in the early 1900s was a crowning achievement in theoretical aerodynamics and validates the mathematical approach of replacing the chord line of the airfoil with a vortex sheet, with the flow tangency condition evaluated along the mean camber line.

This brings to an end our introduction to classical thin airfoil theory. Returning to our road map in Figure 4.7, we have now completed the right-hand branch.

4.9 THE AERODYNAMIC CENTER: ADDITIONAL CONSIDERATIONS

The definition of the aerodynamic center is given in Section 4.3; it is that point on a body about which the aerodynamically generated moment is *independent of angle of attack*. At first thought, it is hard to imagine that such a point could exist. However, the moment coefficient data in Figure 4.11, which are constant with angle of attack, experimentally prove the existence of the aerodynamic center. Moreover, thin airfoil theory as derived in Sections 4.7 and 4.8 clearly shows that, within the assumptions embodied in the theory, not only does the aerodynamic center exist but that it is located at the quarter-chord point on the airfoil. Therefore, to Figure 1.24 which illustrates three different ways of stating the force and moment system on an airfoil, we can now add a fourth way, namely, the specification of the lift and drag acting through the aerodynamic center, and the value of the moment about the aerodynamic center. This is illustrated in Figure 4.29.

For most conventional airfoils, the aerodynamic center is close to, but not necessarily exactly at, the quarter-chord point. Given data for the shape of the

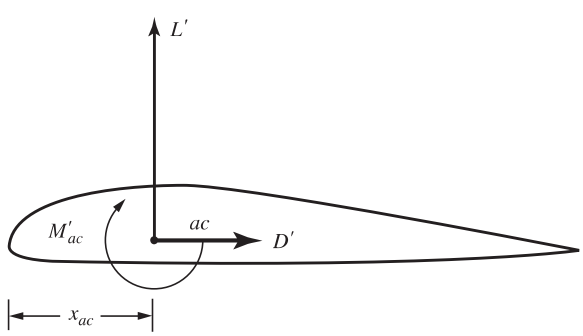

Figure 4.29 Lift, drag, and moments about the aerodynamic center.